

1 **Implementation of trait-based ozone plant sensitivity in the Yale**
2 **Interactive terrestrial Biosphere model v1.0 to assess global vegetation**
3 **damage**

4
5 **Yimian Ma**^{1,2}, **Xu Yue**^{3*}, **Stephen Sitch**^{4*}, **Nadine Unger**³, **Johan Uddling**⁵, **Lina M. Mercado**^{4,6},
6 **Cheng Gong**⁷, **Zhaozhong Feng**⁸, **Huiyi Yang**⁹, **Hao Zhou**^{1,2}, **Chenguang Tian**^{1,2}, **Yang Cao**^{1,2},
7 **Yadong Lei**¹⁰, **Alexander W. Cheesman**^{4,11}, **Yansen Xu**⁸, **Maria Carolina Duran Rojas**¹²

8
9
10 ¹ Climate Change Research Center, Institute of Atmospheric Physics, Chinese Academy of Sciences,
11 Beijing, 100029, China

12 ² University of Chinese Academy of Sciences, Beijing, 100029, China

13 ³ Jiangsu Key Laboratory of Atmospheric Environment Monitoring and Pollution Control, Jiangsu
14 Collaborative Innovation Center of Atmospheric Environment and Equipment Technology, School of
15 Environmental Science and Engineering, Nanjing University of Information Science and Technology,
16 Nanjing, 210044, China

17 ⁴ Faculty of Environment, Science and Economy, University of Exeter, Exeter, EX4 4RJ, UK

18 ⁵ Department of Biological and Environmental Sciences, University of Gothenburg, Gothenburg, P.O.
19 Box 461, 40530, Sweden

20 ⁶ UK Centre for Ecology and Hydrology, Benson Lane, Wallingford, OX10 8BB, UK

21 ⁷ State Key Laboratory of Atmospheric Boundary Layer Physics and Atmospheric Chemistry (LAPC),
22 Institute of Atmospheric Physics, Chinese Academy of Sciences, Beijing, 100029, China

23 ⁸ School of Applied Meteorology, Nanjing University of Information Science and Technology, Nanjing,
24 210044, China

25 ⁹ Livelihoods and Institutions Department, Natural Resources Institute, University of Greenwich, Kent,
26 ME4 4TB, UK

27 ¹⁰ Chinese Academy of Meteorological Sciences, Beijing, 100081, China

28 ¹¹ Centre for Tropical Environmental and Sustainability Science, College of Science & Engineering,
29 James Cook University, Cairns, Queensland, 4870 Australia

30 ¹² College of Engineering, Mathematics, and Physical Sciences, University of Exeter, Exeter, EX4 4PY,
31 UK

32

33 *Correspondence to:* Xu Yue (yuexu@nuist.edu.cn) and Stephen Sitch (S.A.Sitch@exeter.ac.uk)

34

35

36

37

Abstract

38

39 A major limitation in modeling global ozone (O_3) vegetation damage has long been the reliance on
40 empirical O_3 sensitivity parameters derived from a limited number of species and applied at the level of
41 plant functional types (PFTs), which ignore the large interspecific variations within the same PFT. Here,
42 we present a major advance in large-scale assessments of O_3 plant injury by linking the trait leaf mass per
43 area (LMA) and plant O_3 sensitivity in a broad and global perspective. Application of the new approach
44 and a global LMA map in a dynamic global vegetation model reasonably represents the observed
45 interspecific responses to O_3 with a unified sensitivity parameter for all plant species. Simulations suggest
46 a contemporary global mean reduction of 4.8% in gross primary productivity by O_3 , with a range of 1.1%-
47 12.6% for varied PFTs. Hotspots with damages $> 10\%$ are found in agricultural areas in the eastern U.S.,
48 western Europe, eastern China, and India, accompanied by moderate to high levels of surface O_3 .
49 Furthermore, we simulate the distribution of plant sensitivity to O_3 , which is highly linked with the
50 inherent leaf trait trade-off strategies of plants, revealing high risks for fast-growing species with low
51 LMA, such as crops, grasses and deciduous trees.

52

53 **1. Introduction**

54 Tropospheric ozone (O₃) has long been recognized as a hazardous pollutant for plants (Richards et al.,
55 1958; Reich and Amundson, 1985). As a strong oxidant, O₃ can cause damage to leaf cells (Feng et al.,
56 2014), impact stomata conductance (Buker et al., 2015), and reduce photosynthesis and biomass (Wittig
57 et al., 2009). These negative impacts dampen global plant productivity (Ainsworth et al., 2012; Ainsworth
58 et al., 2020) and crop yield (Tai et al., 2014; Emberson et al., 2018; Feng et al., 2022), altering multiple
59 ecosystem functions and services across various spatiotemporal scales (Agathokleous et al., 2020; Feng
60 et al., 2021). Thus, it is of crucial importance to quantify O₃ plant damage in global modeling and assess
61 its coupling effects in the biosphere-atmosphere systems (Zhou et al., 2018).

62

63 To date, O₃ fumigation experiments have been conducted for various plant species. Accordingly, O₃
64 damaging sensitivities, denoted as the Dose-Response Relationships (DRRs), were derived as the
65 regressions between O₃ exposure metrics and the changes in biotic indicators (Mills et al., 2011). The
66 widely-used O₃ metrics include ambient O₃ concentrations for AOT40 (Accumulated O₃ concentration
67 above the Threshold of 40 ppbv (Fuhrer et al., 1997)), or the stomatal O₃ flux for POD_y (Phytotoxic O₃
68 Dose above a threshold flux of y (Buker et al., 2015)). The biotic indicators include visual leaf states,
69 photosynthetic rate, biomass, or crop yield. Normally, the DRRs were derived for typical tree/grass
70 species at specific regions, for example, Norway spruce, birch, and beech in Europe (Buker et al., 2015)
71 or poplar (Shang et al., 2017) and crops (Peng et al., 2019) in East Asia.

72

73 Some assessment studies used DRRs to derive contemporary O₃ plant damage patterns at large scales.
74 Concentration-based DRRs were widely measured and applied on the homogenized land cover, mostly
75 for estimating crop yield loss (Feng et al., 2022; Tai et al., 2021; Hong et al., 2020). However, such DRRs
76 don't include information about biochemical defense and stomatal regulations. Comparatively, flux-based
77 DRRs reflect a more reasonable consideration in biological processes, but are limited by the application
78 scales in both space and time (Mills et al., 2011; Mills et al., 2018b). For example, the estimate of POD_y
79 needs a dry deposition model "DO₃SE" (Deposition of Ozone for Stomatal Exchange) (Clrtap, 2017) or
80 an equivalent model to account for environmental constraints on plant stomatal uptake during the whole

81 growing season. Furthermore, the application of DRRs might introduce uncertainties due to the omission
82 of complex interactions among biotic and abiotic factors at varied spatiotemporal scales.

83

84 Alternatively, more and more mechanistic schemes were developed and implemented in dynamic global
85 vegetation models (DGVMs) to assess the joint effects of environmental factors and O₃ on plants. Felzer
86 et al. (2004) considered both the damaging (through AOT40) and healing (through growth) processes
87 related to O₃ effects within the framework of Terrestrial Ecosystem Model. They further estimated the
88 reduction of 2.6%-6.8% in the net primary productivity by O₃ pollution in U.S. during 1980-1990.
89 Different from Felzer et al. (2004), Sitch et al. (2007) proposed a flux-based scheme linking the
90 instantaneous POD_y with the damaging percentage through the coupling between stomatal conductance
91 and photosynthetic rate. Implementing this scheme into the vegetation model of YIBs, Yue and Unger
92 (2015) predicted a range of 2%-5% reduction in global gross primary productivity (GPP) taking into
93 account the low to high O₃ sensitivities for each vegetation types. Lombardozzi et al. (2015) collected
94 hundreds of measurements and derived the decoupled responses in stomatal conductance and
95 photosynthesis for the same O₃ uptake fluxes. They further implemented the separate response
96 relationships into the Community Land Model and estimated a reduction of 8%-12% in GPP by O₃ at
97 present day. Coupling these schemes with earth system models, studies have assessed interactive O₃
98 impacts on carbon sink (Oliver et al., 2018; Yue and Unger, 2018), global warming (Sitch et al., 2007),
99 and air pollution (Zhou et al., 2018; Gong et al., 2020; Gong et al., 2021; Zhu et al., 2022).

100

101 Although different schemes considered varied physical processes (Ollinger et al., 1997; Felzer et al., 2004;
102 Sitch et al., 2007; Felzer et al., 2009; Lombardozzi et al., 2015; Oliver et al., 2018), they followed the
103 same principle that different O₃ sensitivities should be applied for varied plant functional types (PFTs),
104 as revealed by many measurements in the past four decades (Buker et al., 2015; Mills et al., 2018b) (Table
105 S1). Generally, needleleaf trees, deciduous woody plants, and crop species show ascending sensitivities
106 to O₃ (Reich and Amundson, 1985; Davison and Barnes, 1998; Buker et al., 2015). But the cause of such
107 variation is not fully understood and thus has not been uniformly described in vegetation models
108 (Massman et al., 2000; Tiwari et al., 2016). As a result, all large-scale assessments of O₃ vegetation

109 damage had to rely on a PFT-based range of sensitivity parameters derived from a limited number of plant
110 species and attempted to envelop the range of O₃ impacts by assuming all species within a PFT are either
111 “high” or “low” sensitive to O₃. For example, Felzer et al. (2004) defined empirical sensitivity coefficients
112 for three major plants including deciduous trees, coniferous trees, and crops. In Sitch et al. (2007), the
113 sensitivity coefficients were defined separately for five PFTs with high/low ranges calibrated by DRRs
114 of typical species. These synthesized assumptions cannot resolve the intra-PFT variations in the O₃
115 sensitivity and thus may cause large uncertainties in regional to global assessments.

116

117 Recent observations revealed a uniform plant sensitivity to O₃ if stomatal O₃ flux was expressed based
118 on leaf mass rather than leaf area (Li et al., 2016; Feng et al., 2018; Li et al., 2022). The trait of leaf mass
119 per area (LMA) is an important metric linking leaf area to mass. In a comparative study with 21 woody
120 species (Li et al., 2016) and a meta-analysis of available experimental data (Feng et al., 2018), the DRR
121 showed convergent O₃ sensitivities for conifer and broadleaf trees if the area-based stomatal uptake was
122 converted to the mass-based flux with LMA. This is likely related to the diluting effect of thicker leaves,
123 which normally have stronger defenses against O₃ in their cross-section. Nowadays, a large number of
124 trait observations were synthesized by global networks (Gallagher et al., 2020). The TRY initiative
125 (Kattge et al., 2011) was one of the most influential datasets with 2.3 billion trait data by the year 2021.
126 Based on the TRY dataset, global LMA was estimated with upscaling techniques such as Bayesian
127 modeling (Butler et al., 2017) (thereafter B2017) or the random forest model (Moreno-Martinez et al.,
128 2018) (thereafter M2018). These advances in the retrieval of LMA provide the possibility to depict more
129 accurate O₃ vegetation damage at the global scale.

130

131 Here, we present a major advance in large-scale assessments of O₃ plant damage using a trait-based
132 approach. We implement LMA into a stomatal flux-based O₃ damage framework aiming at a unified
133 representation of plant O₃ sensitivities over the global grids. We couple this new approach to the Yale
134 Interactive terrestrial Biosphere (YIBs) model (Yue and Unger, 2015) and evaluate the derived O₃
135 sensitivities against observations. We further assess contemporary O₃ impacts on global GPP in
136 combination with the recently developed LMA datasets (Butler et al., 2017; Moreno-Martinez et al., 2018;

137 Gallagher et al., 2020) (Fig. 1a) and the multi-model ensemble mean surface O₃ concentrations (Fig. 1b).
138 The updated risk map for O₃ vegetation damage is used to identify the regions and species with the largest
139 sensitivity to O₃ threats.

140

141 2. Scheme development and calibration

142 2.1 The trait-based O₃ vegetation damage scheme

143 We develop the new scheme based on the Sitch et al. (2007) (hereafter S2007) framework for transient
144 O₃ damage calculation. In the original S2007 scheme, the undamaged fraction F for net photosynthetic
145 rate is dependent on the excessive area-based stomatal O₃ flux, which is calculated as the difference
146 between f_{O_3} and PFT-specific area-based threshold y , and modulated by the sensitivity parameter a_{PFT} :

$$147 F = 1 - a_{PFT} \times \max\{f_{O_3} - y, 0\} \quad (1)$$

148 where a_{PFT} is calibrated and varies among PFTs with a typical range from “low” to “high” values
149 indicating uncertainties of plant species within the same PFT. The stomatal O₃ flux f_{O_3} (nmol m⁻² s⁻¹) is
150 calculated as:

$$151 f_{O_3} = \frac{[O_3]}{r + \left[\frac{k_{O_3}}{g_p \times F}\right]} \quad (2)$$

152 where $[O_3]$ is the O₃ concentration at the reference level (nmol m⁻³), r is the aerodynamic and boundary
153 layer resistance between leaf surface and reference level (s m⁻¹). k_{O_3} setting to 1.67 represents the ratio of
154 leaf resistance for O₃ to that for water vapor. g_p represents potential stomata conductance for H₂O (m s⁻¹).
155 ¹).

156

157 Studies suggested that LMA could be used to unify the area-based plant sensitivities to O₃ (Li et al., 2016;
158 Feng et al., 2018), resulting in a constant mass-based parameter a independent of plant species and PFTs:

$$159 a = a_{PFT} \times LMA \quad (3)$$

160 Here, we convert the area-based O₃ stomatal flux expression in Equation (1) to a mass-based flux as
161 follows:

$$162 F = 1 - a \times \max\left\{\frac{f_{O_3}}{LMA} - x, 0\right\} \quad (4)$$

163 where the new sensitivity parameter a is a cross-species constant ($\text{nmol}^{-1} \text{ s g}$); LMA is leaf mass per area
 164 (g m^{-2}); the flux threshold is replaced by a mass-based value of x ($\text{nmol g}^{-1} \text{ s}^{-1}$) (Feng et al., 2018).
 165 Equations (2) and (4) can form a quadratic equation. The F can be derived at each timestep (i.e. hourly)
 166 and applied to net photosynthetic rate and stomatal conductance to calculate the O_3 -induced damages.
 167 The updated LMA-based framework (YIBs-LMA) reduces the number of O_3 sensitivity parameters from
 168 three for each PFT (Sitch et al., 2007) in S2007 to a single parameter a for all PFTs. For YIBs-LMA
 169 framework, the default value of the x threshold in Equation (4) is set to $0.019 \text{ nmol g}^{-1} \text{ s}^{-1}$ as recommended
 170 by Feng et al. (2018).

171

172 **2.2 Dose-response relationship (DRR)**

173 We compare the simulated and observed sensitivities to O_3 so as to calibrate the LMA-based scheme. In
 174 field experiments, DRR is used to quantify species-specific damage by O_3 with a generic format as follows:

$$175 \quad R = 100 + S_O \times \phi_{O_3} \quad (5)$$

176 where R (%) is the relative percentage of a biotic indicator (such as biomass or yield) after and before O_3
 177 damage; ϕ_{O_3} is an area-based O_3 metric (e.g., POD_y measured in sunlit leaves at the top of canopy); S_O
 178 (usually negative) is the observed sensitivity derived as the slope of linear relationship between R and
 179 ϕ_{O_3} . We collected S_O from DRRs with conventional criteria (typically $\text{POD}_{y=1}$ for natural PFTs and
 180 $\text{POD}_{y=6}$ for crops as dose metrics (Clrtap, 2017); the biotic indicators include the relative biomass for
 181 natural PFTs and relative yield for crops) among plant species from International Cooperative Programme
 182 on Effects of Air Pollution on Natural Vegetation and Crops (CLRTAP) (Clrtap, 2017) and multiple
 183 literature sources (Table S1). Such observations are used to calibrate the LMA-based scheme.

184

185 As a comparison with observations, we calculate annual relative GPP percentage (R_{GPP} , %) and POD_y of
 186 sunlit leaves in first canopy layer ($\text{mmol m}^{-2} \text{ year}^{-1}$, based on per leaf area) from the vegetation model to
 187 derive the slopes (S_S) of simulated DRRs. Here, POD_y is a diagnostic variable calculated as:

$$188 \quad \text{POD}_y = \int \max\{f_{O_3} - y, 0\} \quad (6)$$

189 where f_{O_3} represents the stomatal O_3 flux under instant O_3 stimulus at each timestep, which can be
 190 calculated following Equation (2) on the leaf level; y is the prescribed critical level ($1 \text{ nmol m}^{-2} \text{ s}^{-1}$ for

191 natural or $6 \text{ nmol m}^{-2} \text{ s}^{-1}$ for crop species (Clrtap, 2017)). Excessive O_3 flux above y is accumulated for
192 the sunlit leaves of the top canopy layer and over the growing season to derive the POD_y . Simulated S_S is
193 calculated as the slope of the regression between simulated R_{GPP} (%) and POD_y at the PFT level. Only the
194 dominant PFT in each grid is considered for the estimate of S_S at both PFT-level or gridded analyses.

195
196 Similarly, mass-based POD_x is derived from O_3 -impacted f_{O_3} ($\text{nmol m}^{-2} \text{ s}^{-1}$) in Equation (2), together with
197 gridded LMA (g m^{-2}) and mass-based threshold x ($\text{nmol g}^{-1} \text{ s}^{-1}$) as:

$$198 \quad POD_x = \int \left(\frac{f_{\text{O}_3}}{LMA} - x \right) \quad (7)$$

199

200 **2.3 Simulations and calibrations**

201 We perform two groups of supporting experiments (Table 1). The first group explores modeling
202 uncertainties associated with the mass-based framework: (1) YIBs-LMA_B2017 replaces the default
203 LMA map of M2018 (Moreno-Martinez et al., 2018) with B2017 (Butler et al., 2017). (2) YIBs-
204 LMA_PFT applies PFT-specific LMA values (Table S2) for each PFT without considering global LMA
205 geo-gradient. (3) YIBs-LMA_T replaces the default threshold of $x=0.019 \text{ nmol g}^{-1} \text{ s}^{-1}$ with $x=0.006 \text{ nmol}$
206 $\text{g}^{-1} \text{ s}^{-1}$, which is an alternative parameter suggested by observations (Feng et al., 2018). The second group
207 of supporting experiments explores the differences between mass-based and S2007 area-based
208 frameworks. Typically, S2007 has a “low to high” a_{PFT} range for each PFT. Here, a mean sensitivity
209 parameterization of S2007 (YIBs-S2007_adj) is re-calibrated according to S_O in Table S1.

210

211 For all supporting experiments, the parameter a for YIBs-LMA or the eight mean a_{PFT} for YIBs-
212 S2007_adj are derived with the optimal 1:1 fitting between S_S and S_O to minimize the possible biases
213 (Tables 2 and S3-S6). The basic method for calibration is feeding the model with series values of a or
214 a_{PFT} until the predicted O_3 damage matches observations with the lowest normalized mean biases (NMB).
215 For all LMA-based experiments, S_S from varied PFTs were grouped for the calibration of a , while for
216 a_{PFT} in YIBs-S2007_adj, each a_{PFT} is determined individually by matching simulated S_S with S_O . Since
217 S_O are available only for six out of the eight YIBs PFTs, including EBF, NF, DBF, C₃ grass, C₄ grass, and
218 crop (Table S1), S_O of these PFTs are used for calibration. All runs are summarized in Table 1.

219

220 **2.4 YIBs model and forcing data**

221 In this study, all O₃ vegetation damage schemes are implemented in the YIBs model (Yue and Unger,
222 2015), which is a process-based dynamic global vegetation model incorporated with well-established
223 carbon, energy, and water interactive schemes. The model applies the same PFT classifications as the
224 Community Land Model (Bonan et al., 2003) (Fig. S1). Eight PFTs are employed including evergreen
225 broadleaf forest (EBF), needleleaf forest (NF), deciduous broadleaf forest (DBF), cold shrub (C_SHR),
226 arid shrubland (A_SHR), C₃ grassland (C3_GRA), C₄ grassland (C4_GRA), and cropland (CRO) (Fig.
227 S1). For each PFT, phenology is well-evaluated (Yue and Unger, 2015) to generate a reliable growing
228 season, which is crucial for the simulation of stomatal O₃ uptake (Anav et al., 2018). Photosynthesis and
229 stomatal processes are calculated using Farquhar et al. and Ball-Berry algorithms (Farquhar et al., 1980;
230 Ball et al., 1987), respectively. Leaf area index (LAI) and tree height are predicted dynamically based on
231 vegetation carbon allocation. The YIBs model has joined the multi-model ensemble project TRENDY
232 and showed reasonable performance in the simulations of global biomass, GPP, LAI, net ecosystem
233 exchange, and soil carbon relative to observations (Friedlingstein et al., 2020). Key plant biogeochemical
234 parameters of the YIBs model are adjusted for this research (Table S7).

235

236 The hourly modern-era retrospective analysis for research and applications version 2 (MERRA2) climate
237 reanalyses (Gelaro et al., 2017) are used to drive the YIBs model. The gridded LMA required for the main
238 mass-based simulation is derived from Moreno-Martinez et al. (2018) (M2018), which shows the highest
239 value of >150 g m⁻² for needleleaf forest at high latitudes while low values of ~40 g m⁻² for grassland and
240 cropland (Fig. 1a and Fig. S1). Grids with missing LMA data are filled with the mean of the corresponding
241 PFT. Contemporary O₃ concentration fields in the year 2010 from the multi-model mean in Task Force
242 on Hemispheric Transport of Air Pollutants (TF-HTAP) experiments (Turnock et al., 2018) (Fig. 1b) are
243 used as forcing data. The original monthly O₃ data are downscaled to hourly using the diurnal cycle
244 predicted by the chemistry-climate-carbon fully coupled model ModelE2-YIBs (Yue and Unger, 2015).
245 Generally, areas of severe O₃ pollution are found in the mid-latitudes of the Northern Hemisphere with

246 highest annual average O₃ concentration of over 40 ppbv in East Asia. All data are interpolated to the
247 spatial resolution of 1°×1°.

248

249 **3. Results**

250 **3.1 Comparison of simulated sensitivities with observations**

251 Simulated relative GPP percentage (R_{GPP}) at global grids were sorted by dominant PFTs (Fig. S1) and
252 plotted against area-based accumulated phytotoxic O₃ dose above a threshold y nmol m⁻² s⁻¹ ($POD_{y=1}$) at
253 the corresponding grids (Fig. 2). The DRR shows varied slopes among different PFTs, resulting in a
254 coefficient of determination (R^2) around 0.54 for all PFTs (Figs 2a-2c). We further calculated the mass-
255 based accumulated phytotoxic O₃ dose above a threshold of 0.019 nmol g s⁻¹ ($POD_{x=0.019}$) and compared
256 it with R_{GPP} . The updated DRR showed convergent slopes and reached a high R^2 of 0.77 across all PFTs
257 (Figs 2d-2f), suggesting that the mass-based scheme could better unify O₃ sensitivities among different
258 PFTs.

259

260 We then calibrated the single, best-fit a value for the YIBs-LMA framework by minimizing the absolute
261 difference between simulated (S_S) and observed (S_O) slopes of O₃ DRR for all PFTs. With different a
262 parameters, the YIBs-LMA framework yielded considerably high R^2 of ~1.0 but varied biases between
263 simulated and observed O₃ impacts across PFTs (Fig. 3). Both the 1:1 fitting and the lowest bias between
264 S_S and S_O were achieved with an optimal $a = 3.5$ nmol⁻¹ s g (Fig. 3c). Notably, such calibration of a is
265 robust under different O₃ field (see Fig. S2). Consistent with observations, YIBs-LMA with this optimal
266 a parameter simulated low S_S of -0.18% and -0.36% per mmol m⁻² year⁻¹ of $POD_{y=1}$ for evergreen
267 broadleaf forest and needleleaf forest, respectively (Figs 4a, b), median S_S from -0.53% per mmol m⁻²
268 year⁻¹ for arid shrubland (Fig. 4e), and high S_S from -0.64% to -1.04% per mmol m⁻² year⁻¹ for deciduous
269 broadleaf forest, C₃/C₄ grassland, cropland and cold shrubland (-3.28% for crops with $POD_{y=6}$, Figs 4c-
270 d, 4f-h).

271

272 **3.2 Global map of O₃ vegetation damage**

273 We estimated contemporary GPP reductions induced by O₃ with the global concentrations of surface O₃
274 (Fig. 1b) in the year 2010. The YIBs-LMA framework using an increase of *a* parameter yielded an almost
275 linear enhancement of global GPP reduction (Fig. S3) with consistent spatial distributions (Fig. S4). The
276 simulation with the optimal $a = 3.5 \text{ nmol}^{-1} \text{ s g}$ predicted a global GPP reduction of 4.8% (Fig. 5a), which
277 was similar to the value estimated with the area-based S2007 scheme (YIBs-S2007_adj, Table 1). Large
278 reductions of >10% were predicted over the eastern U.S., western Europe, eastern China, and India (Fig.
279 5a). Hotspots were mainly located in cropland and agricultural areas mixed with deciduous broadleaf
280 forest or grassland, accompanied by moderate to high levels of surface O₃. Few discrepancies between
281 the damage maps of YIBs-LMA and YIBs-S007_adj were found (Fig. 5b and Fig. S5), even though the
282 number of parameters was greatly reduced in the YIBs-LMA scheme.

283

284 For YIBs-LMA, PFTs with low LMA such as cropland, grassland, and deciduous broadleaf forest account
285 for 73.3 Pg C yr⁻¹ (50.0%) of the global GPP (Table S8). However, these PFTs contributed to a total GPP
286 reduction of 5.4 Pg C yr⁻¹ (75.5% of total GPP loss) by O₃ damage. In contrast, evergreen broadleaf and
287 needleleaf forests with high LMA accounted for 48.8 Pg C yr⁻¹ (33.0%) of total GPP but yielded only a
288 reduction of 0.75 Pg C yr⁻¹ (10.5% of total GPP loss). Differences in GPP percentage losses were in part
289 associated with the global pattern of O₃ concentrations, which were usually higher over mid-latitudes with
290 populated cities and dense crop plantations (Fig. 1b). However, the differences in LMA and simulated O₃
291 sensitivities of these PFTs also made important contributions to such discrepancies in GPP damages.

292

293 **3.3 Uncertainties of the LMA-based scheme**

294 We quantified the uncertainties of the LMA-based scheme by comparing simulated GPP damages among
295 different experiments (Table 1). The experiment with the alternative LMA map of B2017 (Fig. S6)
296 showed similar spatial patterns but a slightly enhanced GPP reduction of 5.3% (Fig. 6a) compared to the
297 simulations using LMA map of M2018 (Fig. 5a). The B2017 map has a much less source of LMA data
298 than M2018 (~40%), leading to unexpected high O₃ threats over the tundra in the Arctic (Fig. S7). Another
299 experiment using PFT-specific LMA estimated a global GPP reduction of 4.6% (Fig. 6b) with a consistent
300 spatial pattern as the prediction in YIBs-LMA, suggesting that the PFT-level LMA can be used in case of

301 the lack of regional LMA data. The third experiment with an alternative threshold flux (Feng et al., 2018)
302 of $0.006 \text{ nmol g}^{-1} \text{ s}^{-1}$ estimated a high GPP reduction of 6.5% (Fig. 6c) due to the overestimations of O_3
303 sensitivities for some tree PFTs (Fig. 7). The fourth run, YIBs-S2007_adj, predicted a similar global GPP
304 damage of 4.8% as the YIBs-LMA run with a high spatial correlation coefficient of 0.98 (Fig. 6d). Such
305 good consistency is mainly due to the application of recalibrated PFT-level sensitivities in YIBs-
306 S2007_adj. Finally, we tested a new calibration excluding CRO, the PFT that contributed the most to the
307 calibration biases (shown as orange dashed lines in Fig. S8). The results gave an optimal a of 3.2, with
308 global damage of 4.5%. All sensitivity experiments achieved consistent results as the YIBs-LMA
309 simulation with damages ranging from 4.5% to 6.5% and spatial correlation coefficients larger than 0.94.
310

311 **4. Discussion**

312 **4.1 Mechanisms behind the LMA-based approach**

313 In recent decades, the plant science community examined how traits could be used to differentiate and
314 predict the functions of plant species (Reich et al., 1997; Reich et al., 1999). LMA, related to leaf density
315 and thickness, is a key trait reflecting many aspects of leaf function (Reich et al., 1998). In the field of O_3
316 phytotoxicology, experiments have revealed plants with high LMA usually have thick leaves with
317 physical and chemical defenses (Poorter et al., 2009), which can strengthen their resistance to O_3 (Li et
318 al., 2016; Feng et al., 2018). On the contrary, plants with low LMA normally have thin leaves which are
319 likely to be less O_3 -tolerant (Li et al., 2016; Feng et al., 2018). Moreover, it seems plausible that the
320 oxidative stress caused by a given amount of stomatal O_3 flux per unit leaf area would be distributed over
321 a larger leaf mass, and hence diluted, in a leaf with high LMA. Such an LMA- O_3 sensitivity relationship
322 can be well reproduced by our LMA-based model (Figs 8a and 8b). Below we explore the linkage between
323 O_3 plant sensitivities and the mutual adaptation of growth strategies and leaf morphology with plant leaf
324 trade-off theory (Reich et al., 1999; Shipley et al., 2006).

325

326 In the natural world, plants often adapt to maximize carbon uptake under prevailing conditions (Reich et
327 al., 1998; Shipley et al., 2006). To make full use of resources in the growing season, leaves under varied
328 living conditions choose either fast photosynthetic rates (fast-growing deciduous types) or long

329 photosynthesis duration (slow-growing evergreen types) with compatible leaf structures (Reich, 2014;
330 Diaz et al., 2016). The former species expand leaf area (low LMA) to maximize light interception while
331 the latter species produce thick and mechanically strong leaves (high LMA) with ample resistant
332 substances for durable utilization (Poorter et al., 2009) in resource-limited and/or environment-stressed
333 habitats (Wright et al., 2002). As a side effect of such leaf trade-offs, deciduous plants with their high
334 rates of photosynthesis, associated large stomatal conductance (Davison and Barnes, 1998; Henry et al.,
335 2019), and less total defense capacity through the leaf profile (Poorter et al., 2009), are highly O₃ sensitive
336 (Mode1 in Fig. 9). In contrast, the moderate photosynthesis, relatively low maximum stomatal
337 conductance (Davison and Barnes, 1998; Henry et al., 2019), and reinforced dense leaves (Poorter et al.,
338 2009) lead to low sensitivity for evergreen plants (Mode2 in Fig. 9). Therefore, in our modeling practice,
339 the mass-based O₃ gas exchange algorithm can be regarded as taking into account several interrelated
340 factors such as growth-driven gas exchange requirements, gas path length, and biochemical reserves, in
341 a unified, simplified and effective manner via LMA.

342

343 **4.2 Implication of potential risks for fast-growing plants**

344 Our new approach reflected the general experimental findings that deciduous plants are much more
345 vulnerable to O₃ than evergreen species (Li et al., 2017; Feng et al., 2018), and in turn within a PFT,
346 early-successional/pioneers with low LMA are likely more vulnerable than late-successional/canopy trees
347 with high LMA (Fyllas et al., 2012). This law has been neglected in previous modeling studies due to the
348 dependence on the limited observed data used for PFT-specific tuning. Our LMA-based approach bridges
349 this gap through grid-based parameterization, and in addition, our data-model integration specifically
350 emphasizes the broad high risks for fast-growing plants, especially for crops. Among PFTs, crops may
351 endure the largest O₃ threats (Davison and Barnes, 1998; Feng et al., 2021; Mukherjee et al., 2021)
352 because they are artificially bred with high photosynthetic capacities (Richards, 2000), stomatal
353 conductance, generally low LMA (Bertin and Gary, 1998; Wang and Shangguan, 2010; Wu et al., 2018;
354 Li et al., 2018) (roughly 30-60 g m⁻²), and cultivated in populated regions with high ambient O₃
355 concentrations. Modern technology aims to promote crop yield (Herdt, 2005), but this can potentially
356 elevate crop sensitivities to O₃ (Biswas et al., 2008; Biswas et al., 2013). This study estimated the highest

357 annual mean GPP damage for crop, 12.6%, which is at the high end of the 4.4-12.4% of the O₃-induced
358 yield loss estimated for global modeling of soybean, wheat, rice, and maize (Mills et al., 2018a).
359 Furthermore, human-induced land use activities may also increase O₃ damage risks. The global demand
360 for food and commodities leads to the conversion of natural forests to irrigated croplands, grazing pastures,
361 and economical-tree plantations (Curtis et al., 2018; Zalles et al., 2021). Meanwhile, the urgent actions to
362 combat climate change promote large-scale afforestation and reforestation (Cook-Patton et al., 2020).
363 These land use changes with fast-growing plant species may increase the risks of terrestrial ecosystems
364 to surface O₃.

365

366 **4.3 Advances in the global O₃ damage assessment**

367 For the first time, we implemented plant trait LMA into a process-based O₃ impact modeling scheme and
368 obtained reasonable interspecific and inter-PFT O₃ responses supported by observations. The similarity
369 between YIBs-S2007 and YIBs-LMA shown in Fig. 5 revealed an advance in the modeling strategy.
370 Simulated O₃ damage in YIBs-S2007 is based on the PFT-level calibrations that tuned sensitivity
371 parameters of each PFT with observed DRRs. Such refinement is a data-driven approach without clear
372 physical reasons. Instead, the YIBs-LMA framework converts the area-based responses to mass-based
373 ones and achieves better unification in O₃ sensitivities among different PFTs. In this algorithm, the O₃
374 damage efficiency is inversely related to plant LMA, which influences both the O₃ uptake potential and
375 the detoxification capability of the vegetation. The similarity in the global assessment of O₃ vegetation
376 damage between YIBs-S2007 and YIBs-LMA further demonstrated the physical validity of LMA-based
377 scheme in the Earth system modeling, because the independent LMA map was applied in the latter
378 approach.

379

380 In addition to the advance in physical mechanisms, the LMA-based approach improves global O₃ damage
381 assessments in the following aspects. First, it significantly reduces the number of required key parameters.
382 To account for interspecific sensitivities, many schemes have to define PFT-level parameters to cap the
383 ranges of plant responses (Sitch et al., 2007; Felzer et al., 2009; Lombardozzi et al., 2015). As a result,
384 those schemes rely on dozens of parameters which increases the uncertainties of modeling and the

385 difficulties for model calibration. The LMA-based approach requires the calibration of one single
386 parameter a , largely facilitating its application across different vegetation models. Second, the new
387 approach accounts for the continuous spectrum of O₃ sensitivities. Previous studies usually categorized
388 species into groups of low or high O₃ sensitivity, depending on very limited data from O₃ exposure
389 experiments. As a result, gridcells for a specific PFT share the same sensitivities regardless of their
390 geographic locations and ecosystem characteristics. In reality, there are hundreds and thousands of plant
391 species in each PFT and they usually have large variations in biophysical parameters including LMA and
392 O₃ sensitivities. The LMA-based approach takes advantage of the newly revealed unifying concept in O₃
393 sensitivity (Li et al., 2016; Feng et al., 2018; Li et al., 2022) and the recent development in a trait-based
394 LMA global map (Fig. 1a). Such configurations present a spectrum of gridded O₃ sensitivities (Fig. 8a)
395 following the variations of LMA distribution.

396

397 **4.4 Outlook for future modeling**

398 In nature, all aspects of plant physiochemical processes, such as growth, development, reproduction, and
399 defense, are influenced by abiotic factors like water availability, temperature, CO₂ concentration, and
400 light resources (Kochhar and Gujral, 2020). In our modeling, the cumulative O₃ fluxes are based on
401 dynamic plant simulations with well-established DGVM to calculate the effects of these abiotic factors.
402 LMA is considered as a factor representing the vulnerability of each species, by which divergent
403 responses to the same O₃ stomatal dose can be further differentiated. In fact, many other key variables in
404 DGVMs, for example, leaf photosynthetic traits (V_{cmax} and J_{max}), nutrient traits (leaf nitrogen and
405 phosphorus), morphological traits (leaf thickness and size), and phenology-related traits (leaf life span)
406 are all more or less interlinked with LMA (Walker et al., 2014). There are some generic regression
407 relationships between them, which have not yet been fully validated by experimental studies. As a result,
408 considerable improvements can be made in the direction of trait-flexible modeling within the existing
409 DGVM frameworks. Our study demonstrates the validity of LMA-based approach for the O₃ plant
410 damage modeling.

411

412 Although we used the most advanced LMA integrated from available observations, this dataset was
413 developed based on static global grids and revealed the mean state for each pixel. In reality, LMA can
414 vary with biotic/abiotic factors like leaf position in the canopy (Keenan and Niinemets, 2017), phenology,
415 plant health, living environment (Fritz et al., 2018), and climate (Wright et al., 2005; Cui et al., 2020).
416 Even long-term exposure to O₃ can alter leaf morphological characteristics and LMA (Li et al., 2017). In
417 future studies, simulations from local to global scales could implement the spatiotemporal variations in
418 LMA taking into account the demographic information and environmental forcings. We expect a
419 breakthrough in the calculation of reliable LMA to achieve fully dynamic predictions of O₃ plant damage
420 in Earth System Modeling, thus facilitating the research of plant response and adaption in changing
421 environments.

422

423

424 **Code availability**

425 The codes of YIBs model with LMA-based O₃ damaging scheme are shared at
426 <https://zenodo.org/record/6348731>.

427

428 **Data availability**

429 Results of all simulations (listed in Table 1) are available upon request. Data for Figures in the main
430 article are shared at <https://zenodo.org/record/6348731>. The global maps of specific leaf area (SLA) to
431 derive LMA for M2018 and B2017 are from <https://www.try-db.org/TryWeb/Data.php#59> and
432 https://github.com/abhirupdatta/global_maps_of_plant_traits, respectively. Monthly O₃ data is from
433 <https://doi.org/10.5194/acp-18-8953-2018>. Calibration data are summarized in Table S1.

434

435 **Author Contributions**

436 X.Y., S.S. and N.U. designed the research, Y.M.M. performed modeling, data analyses, virtualization and
437 wrote the draft. J.U, L.M., Z.Z.F, and A.W.C advised on concepts and methods. C.G. helped write draft.
438 H.Y.Y., M.C.D.R helped with coding. H.Z., C.G.T., Y.C., Y.D.L., and Y.S.X. helped with data collection.
439 All authors commented and revised the manuscript.

440

441 **Competing interests**

442 The authors declare no conflict of interests.

443

444 **Financial support**

445 Xu Yue acknowledges funding supports from the National Natural Science Foundation of China (grant
446 no. 42275128) and Jiangsu Science Fund for Distinguished Young Scholars (grant no. BK20200040).

447 Yimian Ma acknowledges financial support from China Scholarship Council (CSC no. 201804910712).

448 Johan Uddling acknowledges the strategic research area Biodiversity and Ecosystems in a Changing
449 Climate, BECC. SS, NU, LM, AC were supported by NERC funding (NE/R001812/1).

450

451 **References**

452 Agathokleous, E., Feng, Z., Oksanen, E., Sicard, P., Wang, Q., Saitanis, C. J., Araminiene, V., Blande, J. D., Hayes, F., Calatayud, V.,
453 Domingos, M., Veresoglou, S. D., Penuelas, J., Wardle, D. A., De Marco, A., Li, Z., Harmens, H., Yuan, X., Vitale, M., and Paoletti, E.:
454 Ozone affects plant, insect, and soil microbial communities: A threat to terrestrial ecosystems and biodiversity, *Sci Adv*, 6,
455 10.1126/sciadv.abc1176, 2020.

456 Ainsworth, E. A., Lemonnier, P., and Wedow, J. M.: The influence of rising tropospheric carbon dioxide and ozone on plant productivity,
457 *Plant Biology*, 22, 5-11, 10.1111/plb.12973, 2020.

458 Ainsworth, E. A., Yendrek, C. R., Sitch, S., Collins, W. J., and Emberson, L. D.: The Effects of Tropospheric Ozone on Net Primary
459 Productivity and Implications for Climate Change, *Annu Rev Plant Biol*, 63, 637-661, 10.1146/Annurev-Arplant-042110-103829, 2012.

460 Anav, A., Liu, Q., De Marco, A., Proietti, C., Savi, F., Paoletti, E., and Piao, S.: The role of plant phenology in stomatal ozone flux modeling,
461 *Global Change Biol*, 24, 235-248, 10.1111/gcb.13823, 2018.

462 Ball, J. T., Woodrow, I. E., and Berry, J. A.: A model predicting stomatal conductance and its contribution to the control of photosynthesis
463 under different environmental conditions, *Progress in Photosynthesis Research: Viith International Congress on Photosynthesis*,
464 10.1007/978-94-017-0519-6_48, 1987.

465 Bertin, N. and Gary, C.: Short and long term fluctuations of the leaf mass per area of tomato plants - Implications for growth models, *Ann*
466 *Bot-London*, 82, 71-81, DOI 10.1006/anbo.1998.0647, 1998.

467 Biswas, D. K., Xu, H., Li, Y. G., Ma, B. L., and Jiang, G. M.: Modification of photosynthesis and growth responses to elevated CO₂ by
468 ozone in two cultivars of winter wheat with different years of release, *J Exp Bot*, 64, 1485-1496, 10.1093/jxb/ert005, 2013.

469 Biswas, D. K., Xu, H., Li, Y. G., Sun, J. Z., Wang, X. Z., Han, X. G., and Jiang, G. M.: Genotypic differences in leaf biochemical,
470 physiological and growth responses to ozone in 20 winter wheat cultivars released over the past 60 years, *Global Change Biol*, 14, 46-59,
471 10.1111/j.1365-2486.2007.01477.x, 2008.

472 Bonan, G. B., Levis, S., Sitch, S., Vertenstein, M., and Oleson, K. W.: A dynamic global vegetation model for use with climate models:
473 concepts and description of simulated vegetation dynamics, *Global Change Biol*, 9, 1543-1566, 10.1046/J.1365-2486.2003.00681.X, 2003.

474 Buker, P., Feng, Z., Uddling, J., Briolat, A., Alonso, R., Braun, S., Elvira, S., Gerosa, G., Karlsson, P. E., Le Thiec, D., Marzuoli, R., Mills,
475 G., Oksanen, E., Wieser, G., Wilkinson, M., and Emberson, L. D.: New flux based dose-response relationships for ozone for European forest
476 tree species, *Environ Pollut*, 206, 163-174, 10.1016/j.envpol.2015.06.033, 2015.

477 Butler, E. E., Datta, A., Flores-Moreno, H., Chen, M., Wythers, K. R., Fazayeli, F., Banerjee, A., Atkin, O. K., Kattge, J., Amiaud, B.,
478 Blonder, B., Boenisch, G., Bond-Lamberty, B., Brown, K. A., Byun, C., Campetella, G., Cerabolini, B. E. L., Cornelissen, J. H. C., Craine,
479 J. M., Craven, D., de Vries, F. T., Diaz, S., Domingues, T. F., Forey, E., Gonzalez-Melo, A., Gross, N., Han, W., Hattingh, W. N., Hickler,
480 T., Jansen, S., Kramer, K., Kraft, N. J. B., Kurokawa, H., Laughlin, D. C., Meir, P., Minden, V., Niinemets, U., Onoda, Y., Penuelas, J.,
481 Read, Q., Sack, L., Schamp, B., Soudzilovskaia, N. A., Spasojevic, M. J., Sosinski, E., Thornton, P. E., Valladares, F., van Bodegom, P. M.,
482 Williams, M., Wirth, C., and Reich, P. B.: Mapping local and global variability in plant trait distributions, *Proc Natl Acad Sci U S A*, 114,
483 E10937-E10946, 10.1073/pnas.1708984114, 2017.

484 CLRTAP: The UNECE Convention on Long-range Transboundary Air Pollution, Manual on Methodologies and Criteria for Modelling and
485 Mapping Critical Loads and Levels and Air Pollution Effects, Risks and Trends: Chapter III Mapping Critical Levels for Vegetation, 2017.

486 Cook-Patton, S. C., Leavitt, S. M., Gibbs, D., Harris, N. L., Lister, K., Anderson-Teixeira, K. J., Briggs, R. D., Chazdon, R. L., Crowther,
487 T. W., Ellis, P. W., Griscom, H. P., Herrmann, V., Holl, K. D., Houghton, R. A., Larrosa, C., Lomax, G., Lucas, R., Madsen, P., Malhi, Y.,
488 Paquette, A., Parker, J. D., Paul, K., Routh, D., Roxburgh, S., Saatchi, S., van den Hoogen, J., Walker, W. S., Wheeler, C. E., Wood, S. A.,
489 Xu, L., and Griscom, B. W.: Mapping carbon accumulation potential from global natural forest regrowth, *Nature*, 585, 545-550,
490 10.1038/s41586-020-2686-x, 2020.

491 Cui, E., Weng, E., Yan, E., and Xia, J.: Robust leaf trait relationships across species under global environmental changes, *Nat Commun*, 11,
492 2999, 10.1038/s41467-020-16839-9, 2020.

493 Curtis, P. G., Slay, C. M., Harris, N. L., Tyukavina, A., and Hansen, M. C.: Classifying drivers of global forest loss, *Science*, 361, 1108-
494 1111, 10.1126/science.aau3445, 2018.

495 Davison, A. W. and Barnes, J. D.: Effects of ozone on wild plants, *New Phytol*, 139, 135-151, <https://doi.org/10.1046/j.1469-8137.1998.00177.x>, 1998.

497 Diaz, S., Kattge, J., Cornelissen, J. H., Wright, I. J., Lavorel, S., Dray, S., Reu, B., Kleyer, M., Wirth, C., Prentice, I. C., Garnier, E., Bonisch,
498 G., Westoby, M., Poorter, H., Reich, P. B., Moles, A. T., Dickie, J., Gillison, A. N., Zanne, A. E., Chave, J., Wright, S. J., Sheremet'ev, S.
499 N., Jactel, H., Baraloto, C., Cerabolini, B., Pierce, S., Shipley, B., Kirkup, D., Casanoves, F., Joswig, J. S., Gunther, A., Falczuk, V., Ruger,
500 N., Mahecha, M. D., and Gorne, L. D.: The global spectrum of plant form and function, *Nature*, 529, 167-171, 10.1038/nature16489, 2016.

501 Emberson, L. D., Pleijel, H., Ainsworth, E. A., van den Berg, M., Ren, W., Osborne, S., Mills, G., Pandey, D., Dentener, F., Buker, P., Ewert,
502 F., Koeble, R., and Van Dingenen, R.: Ozone effects on crops and consideration in crop models, *Eur J Agron*, 100, 19-34,
503 10.1016/j.eja.2018.06.002, 2018.

504 Farquhar, G. D., Caemmerer, S. V., and Berry, J. A.: A biochemical-model of photosynthetic CO₂ assimilation in leaves of C3 Species,
505 *Planta*, 149, 78-90, 10.1007/Bf00386231, 1980.

506 Felzer, B., Kicklighter, D., Melillo, J., Wang, C., Zhuang, Q., and Prinn, R.: Effects of ozone on net primary production and carbon
507 sequestration in the conterminous United States using a biogeochemistry model, *Tellus B*, 56, 230-248, <https://doi.org/10.1111/j.1600-0889.2004.00097.x>, 2004.

508 Felzer, B. S., Cronin, T. W., Melillo, J. M., Kicklighter, D. W., and Schlosser, C. A.: Importance of carbon-nitrogen interactions and ozone
509 on ecosystem hydrology during the 21st century, *J. Geophys. Res.*, 114, G01020, 10.1029/2008jg000826, 2009.

510 Feng, Z., Xu, Y., Kobayashi, K., Dai, L., Zhang, T., Agathokleous, E., Calatayud, V., Paoletti, E., Mukherjee, A., Agrawal, M., Park, R. J.,
511 Oak, Y. J., and Yue, X.: Ozone pollution threatens the production of major staple crops in East Asia, *Nature Food*, 3, 47-56, 10.1038/s43016-
512 021-00422-6, 2022.

514 Feng, Z., Agathokleous, E., Yue, X., Oksanen, E., Paoletti, E., Sase, H., Gandin, A., Koike, T., Calatayud, V., Yuan, X., Liu, X., De Marco,
515 A., Jolivet, Y., Kontunen-Soppela, S., Hoshika, Y., Saji, H., Li, P., Li, Z., Watanabe, M., and Kobayashi, K.: Emerging challenges of ozone
516 impacts on asian plants: actions are needed to protect ecosystem health, *Ecosystem Health and Sustainability*, 7, 1911602,
517 10.1080/20964129.2021.1911602, 2021.

518 Feng, Z. Z., Sun, J. S., Wan, W. X., Hu, E. Z., and Calatayud, V.: Evidence of widespread ozone-induced visible injury on plants in Beijing,
519 China, *Environ Pollut*, 193, 296-301, 10.1016/j.envpol.2014.06.004, 2014.

520 Feng, Z. Z., Buker, P., Pleijel, H., Emberson, L., Karlsson, P. E., and Uddling, J.: A unifying explanation for variation in ozone sensitivity
521 among woody plants, *Glob. Change Biol.*, 24, 78-84, 10.1111/gcb.13824, 2018.

522 Fritz, M. A., Rosa, S., and Sicard, A.: Mechanisms Underlying the Environmentally Induced Plasticity of Leaf Morphology, *Front Genet*, 9,
523 478, 10.3389/fgene.2018.00478, 2018.

524 Fuhrer, J., Skarby, L., and Ashmore, M. R.: Critical levels for ozone effects on vegetation in Europe, *Environ Pollut*, 97, 91-106,
525 10.1016/s0269-7491(97)00067-5, 1997.

526 Fyllas, N. M., Quesada, C. A., and Lloyd, J.: Deriving Plant Functional Types for Amazonian forests for use in vegetation dynamics models,
527 *Perspectives in Plant Ecology, Evolution and Systematics*, 14, 97-110, <https://doi.org/10.1016/j.ppees.2011.11.001>, 2012.

528 Gallagher, R. V., Falster, D. S., Maitner, B. S., Salguero-Gomez, R., Vandvik, V., Pearse, W. D., Schneider, F. D., Kattge, J., Poelen, J. H.,
529 Madin, J. S., Ankenbrand, M. J., Penone, C., Feng, X., Adams, V. M., Alroy, J., Andrew, S. C., Balk, M. A., Bland, L. M., Boyle, B. L.,
530 Bravo-Avila, C. H., Brennan, L., Carthey, A. J. R., Catullo, R., Cavazos, B. R., Conde, D. A., Chown, S. L., Fadrique, B., Gibb, H., Halbritter,
531 A. H., Hammock, J., Hogan, J. A., Holewa, H., Hope, M., Iversen, C. M., Jochum, M., Kearney, M., Keller, A., Mabee, P., Manning, P.,
532 McCormack, L., Michaletz, S. T., Park, D. S., Perez, T. M., Pineda-Munoz, S., Ray, C. A., Rossetto, M., Sauquet, H., Sparrow, B., Spasojevic,
533 M. J., Telford, R. J., Tobias, J. A., Violle, C., Walls, R., Weiss, K. C. B., Westoby, M., Wright, I. J., and Enquist, B. J.: Open Science
534 principles for accelerating trait-based science across the Tree of Life, *Nat Ecol Evol*, 4, 294-303, 10.1038/s41559-020-1109-6, 2020.

535 Gelaro, R., McCarty, W., Suarez, M. J., Todling, R., Molod, A., Takacs, L., Randles, C. A., Darmenov, A., Bosilovich, M. G., Reichle, R.,
536 Wargan, K., Coy, L., Cullather, R., Draper, C., Akella, S., Buchard, V., Conaty, A., da Silva, A. M., Gu, W., Kim, G.-K., Koster, R., Lucchesi,
537 R., Merkova, D., Nielsen, J. E., Partyka, G., Pawson, S., Putman, W., Rienecker, M., Schubert, S. D., Sienkiewicz, M., and Zhao, B.: The
538 Modern-Era Retrospective Analysis for Research and Applications, Version 2 (MERRA-2), *J Climate*, 30, 5419-5454, 10.1175/jcli-d-16-
539 0758.1, 2017.

540 Gong, C., Lei, Y., Ma, Y., Yue, X., and Liao, H.: Ozone–vegetation feedback through dry deposition and isoprene emissions in a global
541 chemistry–carbon–climate model, *Atmos. Chem. Phys.*, 20, 3841-3857, 10.5194/acp-20-3841-2020, 2020.

542 Gong, C., Liao, H., Yue, X., Ma, Y., and Lei, Y.: Impacts of Ozone-Vegetation Interactions on Ozone Pollution Episodes in North China
543 and the Yangtze River Delta, *Geophys Res Lett*, 48, 10.1029/2021gl093814, 2021.

544 Henry, C., John, G. P., Pan, R., Bartlett, M. K., Fletcher, L. R., Scoffoni, C., and Sack, L.: A stomatal safety-efficiency trade-off constrains
545 responses to leaf dehydration, *Nat Commun*, 10, 3398, 10.1038/s41467-019-11006-1, 2019.

546 Herdt, R. W.: The state of food and agriculture, 2003-2004: Agricultural biotechnology: Meeting the needs of the poor?, *Agricultural
547 Economics*, 32, 109-+, 10.1111/j.0169-5150.2005.t01-7-00008.x, 2005.

548 Hong, C., Mueller, N. D., Burney, J. A., Zhang, Y., AghaKouchak, A., Moore, F. C., Qin, Y., Tong, D., and Davis, S. J.: Impacts of ozone
549 and climate change on yields of perennial crops in California, *Nature Food*, 1, 166-172, 10.1038/s43016-020-0043-8, 2020.

550 Kattge, J., Diaz, S., Lavorel, S., Prentice, C., Leadley, P., Bonisch, G., Garnier, E., Westoby, M., Reich, P. B., Wright, I. J., Cornelissen, J.
551 H. C., Violle, C., Harrison, S. P., van Bodegom, P. M., Reichstein, M., Enquist, B. J., Soudzilovskaia, N. A., Ackerly, D. D., Anand, M.,
552 Atkin, O., Bahn, M., Baker, T. R., Baldocchi, D., Bekker, R., Blanco, C. C., Blonder, B., Bond, W. J., Bradstock, R., Bunker, D. E.,
553 Casanoves, F., Cavender-Bares, J., Chambers, J. Q., Chapin, F. S., Chave, J., Coomes, D., Cornwell, W. K., Craine, J. M., Dobrin, B. H.,
554 Duarte, L., Durka, W., Elser, J., Esser, G., Estiarte, M., Fagan, W. F., Fang, J., Fernandez-Mendez, F., Fidelis, A., Finegan, B., Flores, O.,
555 Ford, H., Frank, D., Freschet, G. T., Fyllas, N. M., Gallagher, R. V., Green, W. A., Gutierrez, A. G., Hickler, T., Higgins, S. I., Hodgson, J.
556 G., Jalili, A., Jansen, S., Joly, C. A., Kerkhoff, A. J., Kirkup, D., Kitajima, K., Kleyer, M., Klotz, S., Knops, J. M. H., Kramer, K., Kuhn, I.,
557 Kurokawa, H., Laughlin, D., Lee, T. D., Leishman, M., Lens, F., Lenz, T., Lewis, S. L., Lloyd, J., Llusia, J., Louault, F., Ma, S., Mahecha,
558 M. D., Manning, P., Massad, T., Medlyn, B. E., Messier, J., Moles, A. T., Muller, S. C., Nadrowski, K., Naeem, S., Niinemets, U., Nollert,
559 S., Nuske, A., Ogaya, R., Oleksyn, J., Onipchenko, V. G., Onoda, Y., Ordóñez, J., Overbeck, G., Ozinga, W. A., Patino, S., Paula, S., Pausas,
560 J. G., Penuelas, J., Phillips, O. L., Pillar, V., Poorter, H., Poorter, L., Poschlod, P., Prinzing, A., Proulx, R., Rammig, A., Reinsch, S., Reu,
561 B., Sack, L., Salgado-Negre, B., Sardans, J., Shiodera, S., Shipley, B., Siefert, A., Sosinski, E., Soussana, J. F., Swaine, E., Swenson, N.,
562 Thompson, K., Thornton, P., Waldram, M., Weiher, E., White, M., White, S., Wright, S. J., Yguel, B., Zaehle, S., Zanne, A. E., and Wirth,
563 C.: TRY - a global database of plant traits, *Global Change Biol*, 17, 2905-2935, Doi 10.1111/J.1365-2486.2011.02451.X, 2011.

564 Keenan, T. F. and Niinemets, U.: Global leaf trait estimates biased due to plasticity in the shade, *Nat Plants*, 3, ARTN 16201
565 10.1038/nplants.2016.201, 2017.

566 Kochhar, S. and Gujral, S.: Abiotic and Biotic Stress, in: *Plant Physiology: Theory and Applications*, 2 ed., edited by: Kochhar, S. L., and
567 Gujral, S. K., Cambridge University Press, Cambridge, 545-589, DOI: 10.1017/9781108486392.021, 2020.

568 Li, D., Wang, X., Zheng, H., Zhou, K., Yao, X., Tian, Y., Zhu, Y., Cao, W., and Cheng, T.: Estimation of area- and mass-based leaf nitrogen
569 contents of wheat and rice crops from water-removed spectra using continuous wavelet analysis, *Plant Methods*, 14, 10.1186/s13007-018-
570 0344-1, 2018.

571 Li, P., Calatayud, V., Gao, F., Uddling, J., and Feng, Z. Z.: Differences in ozone sensitivity among woody species are related to leaf
572 morphology and antioxidant levels, *Tree Physiol.*, 36, 1105-1116, 10.1093/treephys/tpw042, 2016.

573 Li, P., Feng, Z., Catalayud, V., Yuan, X., Xu, Y., and Paoletti, E.: A meta-analysis on growth, physiological, and biochemical responses of
574 woody species to ground-level ozone highlights the role of plant functional types, *Plant Cell Environ*, 40, 2369-2380, 10.1111/pce.13043,
575 2017.

576 Li, S., Moller, C. A., Mitchell, N. G., Lee, D., Sacks, E. J., and Ainsworth, E. A.: Testing unified theories for ozone response in C-4 species,
577 *Global Change Biol*, 28, 3379-3393, 10.1111/gcb.16108, 2022.

578 Lombardozzi, D., Levis, S., Bonan, G., Hess, P. G., and Sparks, J. P.: The Influence of Chronic Ozone Exposure on Global Carbon and
579 Water Cycles, *J Climate*, 28, 292-305, 10.1175/Jcli-D-14-00223.1, 2015.

580 Massman, W. J., Musselman, R. C., and Lefohn, A. S.: A conceptual ozone dose-response model to develop a standard to protect vegetation,
581 *Atmos Environ*, 34, 745-759, 10.1016/s1352-2310(99)00395-7, 2000.

582 Mills, G., Hayes, F., Simpson, D., Emberson, L., Norris, D., Harmens, H., and Buker, P.: Evidence of widespread effects of ozone on crops
583 and (semi-)natural vegetation in Europe (1990-2006) in relation to AOT40-and flux-based risk maps, *Global Change Biol*, 17, 592-613,
584 10.1111/j.1365-2486.2010.02217.x, 2011.

585 Mills, G., Sharps, K., Simpson, D., Pleijel, H., Frei, M., Burkey, K., Emberson, L., Uddling, J., Broberg, M., Feng, Z., Kobayashi, K., and
586 Agrawal, M.: Closing the global ozone yield gap: Quantification and cobenefits for multistress tolerance, *Glob Chang Biol*, 24, 4869-4893,
587 10.1111/gcb.14381, 2018a.

588 Mills, G., Sharps, K., Simpson, D., Pleijel, H., Broberg, M., Uddling, J., Jaramillo, F., Davies, W. J., Dentener, F., Van den Berg, M.,
589 Agrawal, M., Agrawal, S. B., Ainsworth, E. A., Buker, P., Emberson, L., Feng, Z. Z., Harmens, H., Hayes, F., Kobayashi, K., Paoletti, E.,
590 and Van Dingenen, R.: Ozone pollution will compromise efforts to increase global wheat production, *Global Change Biol*, 24, 3560-3574,
591 10.1111/gcb.14157, 2018b.

592 Moreno-Martinez, A., Camps-Valls, G., Kattge, J., Robinson, N., Reichstein, M., van Bodegom, P., Kramer, K., Cornelissen, J. H. C., Reich,
593 P., Bahn, M., Niinemets, U., Penuelas, J., Craine, J. M., Cerabolini, B. E. L., Minden, V., Laughlin, D. C., Sack, L., Allred, B., Baraloto, C.,
594 Byun, C., Soudzilovskaia, N. A., and Running, S. W.: A methodology to derive global maps of leaf traits using remote sensing and climate
595 data, *Remote Sens Environ*, 218, 69-88, 2018.

596 Mukherjee, A., Yadav, D. S., Agrawal, S. B., and Agrawal, M.: Ozone a persistent challenge to food security in India: Current status and
597 policy implications, *Current Opinion in Environmental Science & Health*, 19, 100220, <https://doi.org/10.1016/j.coesh.2020.10.008>, 2021.

598 Oliver, R. J., Mercado, L. M., Sitch, S., Simpson, D., Medlyn, B. E., Lin, Y. S., and Folberth, G. A.: Large but decreasing effect of ozone
599 on the European carbon sink, *Biogeosciences*, 15, 4245-4269, 10.5194/bg-15-4245-2018, 2018.

600 Ollinger, S. V., Aber, J. D., and Reich, P. B.: Simulating Ozone Effects on Forest Productivity: Interactions among Leaf-, Canopy-, and
601 Stand-Level Processes, *Ecol Appl*, 7, 1237-1251, 10.2307/2641211, 1997.

602 Peng, J. L., Shang, B., Xu, Y. S., Feng, Z. Z., Pleijel, H., and Calatayud, V.: Ozone exposure- and flux-yield response relationships for maize,
603 *Environ Pollut*, 252, 1-7, 2019.

604 Poorter, H., Niinemets, U., Poorter, L., Wright, I. J., and Villar, R.: Causes and consequences of variation in leaf mass per area (LMA): a
605 meta-analysis, *New Phytol*, 182, 565-588, 10.1111/j.1469-8137.2009.02830.x, 2009.

606 Reich, P. B.: The world-wide 'fast-slow' plant economics spectrum: a traits manifesto, *J Ecol*, 102, 275-301, 10.1111/1365-2745.12211,
607 2014.

608 Reich, P. B. and Amundson, R. G.: AMBIENT LEVELS OF OZONE REDUCE NET PHOTOSYNTHESIS IN TREE AND CROP
609 SPECIES, *Science*, 230, 566-570, 10.1126/science.230.4725.566, 1985.

610 Reich, P. B., Ellsworth, D. S., and Walters, M. B.: Leaf structure (specific leaf area) modulates photosynthesis-nitrogen relations: evidence
611 from within and across species and functional groups, *Funct Ecol*, 12, 948-958, DOI 10.1046/j.1365-2435.1998.00274.x, 1998.

612 Reich, P. B., Walters, M. B., and Ellsworth, D. S.: From tropics to tundra: Global convergence in plant functioning, *P Natl Acad Sci USA*,
613 94, 13730-13734, 10.1073/pnas.94.25.13730, 1997.

614 Reich, P. B., Ellsworth, D. S., Walters, M. B., Vose, J. M., Gresham, C., Volin, J. C., and Bowman, W. D.: Generality of leaf trait
615 relationships: A test across six biomes, *Ecology*, 80, 1955-1969, 10.1890/0012-9658(1999)080[1955:goltra]2.0.co;2, 1999.

616 Richards, B. L., Middleton, J. T., and Hewitt, W. B.: Air Pollution With Relation to Agronomic Crops: V. Oxidant Stipple of Grape, *Agron*
617 *J*, 50, 559-561, 1958.

618 Richards, R. A.: Selectable traits to increase crop photosynthesis and yield of grain crops, *J Exp Bot*, 51, 447-458,
619 10.1093/jexbot/51.suppl_1.447, 2000.

620 Shang, B., Feng, Z. Z., Li, P., Yuan, X. Y., Xu, Y. S., and Calatayud, V.: Ozone exposure- and flux-based response relationships with
621 photosynthesis, leaf morphology and biomass in two poplar clones, *Sci Total Environ*, 603, 185-195, 10.1016/j.scitotenv.2017.06.083, 2017.

622 Shipley, B., Lechowicz, M. J., Wright, I., and Reich, P. B.: Fundamental trade-offs generating the worldwide leaf economics spectrum,
623 *Ecology*, 87, 535-541, 10.1890/05-1051, 2006.

624 Sitch, S., Cox, P. M., Collins, W. J., and Huntingford, C.: Indirect radiative forcing of climate change through ozone effects on the land-
625 carbon sink, *Nature*, 448, 791-794, 10.1038/Nature06059, 2007.

626 Tai, A. P. K., Martin, M. V., and Heald, C. L.: Threat to future global food security from climate change and ozone air pollution, *Nat Clim*
627 *Change*, 4, 817-821, 10.1038/nclimate2317, 2014.

628 Tai, A. P. K., Sadiq, M., Pang, J. Y. S., Yung, D. H. Y., and Feng, Z.: Impacts of Surface Ozone Pollution on Global Crop Yields: Comparing
629 Different Ozone Exposure Metrics and Incorporating Co-effects of CO₂, *Frontiers in Sustainable Food Systems*, 5,
630 10.3389/fsufs.2021.534616, 2021.

631 Tiwari, S., Grote, R., Churkina, G., and Butler, T.: Ozone damage, detoxification and the role of isoprenoids - new impetus for integrated
632 models, *Funct Plant Biol*, 43, 324-336, 10.1071/fp15302, 2016.

633 Turnock, S. T., Wild, O., Dentener, F. J., Davila, Y., Emmons, L. K., Flemming, J., Folberth, G. A., Henze, D. K., Jonson, J. E., Keating, T.
634 J., Kengo, S., Lin, M., Lund, M., Tilmes, S., and O'Connor, F. M.: The impact of future emission policies on tropospheric ozone using a
635 parameterized approach, *Atmos Chem Phys*, 18, 8953-8978, 10.5194/acp-18-8953-2018, 2018.

636 Walker, A. P., Beckerman, A. P., Gu, L., Kattge, J., Cernusak, L. A., Domingues, T. F., Scales, J. C., Wohlfahrt, G., Wullschleger, S. D.,
637 and Woodward, F. I.: The relationship of leaf photosynthetic traits – V_{cmax} and J_{max} – to leaf nitrogen, leaf phosphorus, and specific leaf
638 area: a meta-analysis and modeling study, *Ecol Evol*, 4, 3218-3235, <https://doi.org/10.1002/ece3.1173>, 2014.

639 Wang, K. and Shangguan, Z.: Photosynthetic characteristics and resource utilization efficiency of maize (*Zea mays*L.) and millet (*Setaria*
640 *italica*L.) in a semi-arid hilly loess region in China, *New Zeal J Crop Hort*, 38, 247-254, 10.1080/01140671.2010.503987, 2010.

641 Wittig, V. E., Ainsworth, E. A., Naidu, S. L., Karnosky, D. F., and Long, S. P.: Quantifying the impact of current and future tropospheric
642 ozone on tree biomass, growth, physiology and biochemistry: a quantitative meta-analysis, *Global Change Biol*, 15, 396-424, 2009.

643 Wright, I. J., Westoby, M., and Reich, P. B.: Convergence towards higher leaf mass per area in dry and nutrient-poor habitats has different
644 consequences for leaf life span, *J Ecol*, 90, 534-543, 10.1046/j.1365-2745.2002.00689.x, 2002.

645 Wright, I. J., Reich, P. B., Cornelissen, J. H. C., Falster, D. S., Groom, P. K., Hikosaka, K., Lee, W., Lusk, C. H., Niinemets, U., Oleksyn,
646 J., Osada, N., Poorter, H., Warton, D. I., and Westoby, M.: Modulation of leaf economic traits and trait relationships by climate, *Global Ecol*
647 *Biogeogr*, 14, 411-421, 10.1111/j.1466-822x.2005.00172.x, 2005.

648 Wu, Y., Gong, W., Wang, Y., Yong, T., Yang, F., Liu, W., Wu, X., Du, J., Shu, K., Liu, J., Liu, C., and Yang, W.: Leaf area and
649 photosynthesis of newly emerged trifoliolate leaves are regulated by mature leaves in soybean, *J Plant Res*, 131, 671-680, 10.1007/s10265-
650 018-1027-8, 2018.

651 Yue, X. and Unger, N.: The Yale Interactive terrestrial Biosphere model version 1.0: description, evaluation and implementation into NASA
652 GISS ModelE2, *Geosci Model Dev*, 8, 2399-2417, 10.5194/gmd-8-2399-2015, 2015.

653 Yue, X. and Unger, N.: Fire air pollution reduces global terrestrial productivity, *Nat Commun*, 9, 5413, 2018.

654 Zalles, V., Hansen, M. C., Potapov, P. V., Parker, D., Stehman, S. V., Pickens, A. H., Parente, L. L., Ferreira, L. G., Song, X.-P., Hernandez-
655 Serna, A., and Kommareddy, I.: Rapid expansion of human impact on natural land in South America since 1985, *Sci Adv*, 7, eabg1620,
656 10.1126/sciadv.abg1620, 2021.

657 Zhou, S. S., Tai, A. P. K., Sun, S., Sadiq, M., Heald, C. L., and Geddes, J. A.: Coupling between surface ozone and leaf area index in a
658 chemical transport model: strength of feedback and implications for ozone air quality and vegetation health, *Atmos. Chem. Phys.*, 18, 14133-
659 14148, 10.5194/acp-18-14133-2018, 2018.

660 Zhu, J., Tai, A. P. K., and Hung Lam Yim, S.: Effects of ozone–vegetation interactions on meteorology and air quality in China using a two-
661 way coupled land–atmosphere model, *Atmos. Chem. Phys.*, 22, 765-782, 10.5194/acp-22-765-2022, 2022.

662

663

664 **Table 1.** Summary of simulations.

665

Experiment ^a	Method	Thresholds ^a (<i>x</i> or <i>y</i>)	LMA format	LMA map	Optimal (<i>a</i> or <i>a_{PFT}</i>)	Tests (<i>a</i> or <i>a_{PFT}</i>)
YIBs-LMA		<i>x</i> =0.019	gridded	M2018	<i>a</i> =3.5 (Table 2)	five tests (<i>a</i> =2.5, 3, 3.5, 4, 4.5)
YIBs-LMA_PFT	Mass- based	<i>x</i> =0.019	PFT- specific	M2018	<i>a</i> =2.0 (Table S3)	five tests (<i>a</i> =2, 2.5, 3, 3.5, 4)
YIBs-LMA_T		<i>x</i> =0.006	gridded	M2018	<i>a</i> =3.0 (Table S4)	five tests (<i>a</i> =2, 2.5, 3, 3.5, 4)
YIBs-LMA_B2017		<i>x</i> =0.019	gridded	B2017	<i>a</i> =2.8 (Table S5)	five tests (<i>a</i> =2, 2.5, 2.8, 3, 3.5)
YIBs-S2007_adj	Area- based	8 values for <i>y</i> (Table S6)	/	/	8 values for <i>a_{PFT}</i> (Table S6)	40 tests (five each for 8 PFTs)

666

667 ^a Units of thresholds are nmol g⁻¹ s⁻¹ for *x* and nmol m⁻² s⁻¹ for *y*668 ^b Units of key parameters are nmol⁻¹ s g for *a* and nmol⁻¹ m² s for *a_{PFT}*

669

670 **Table 2.** Calibrations of the YIBs-LMA ^a experiment with varied *a*.

671

PFT	S_o						S_s/S_o ^b				
	a=2.5	a=3.0	a=3.5	a=4.0	a=4.5		a=2.5	a=3.0	a=3.5	a=4.0	a=4.5
EBF	-0.19	-0.13	-0.16	-0.18	-0.21	-0.23	0.70	0.83	0.96	1.08	1.20
NF	-0.23	-0.26	-0.31	-0.36	-0.40	-0.45	1.14	1.35	1.56	1.75	1.95
DBF	-0.70	-0.51	-0.60	-0.69	-0.78	-0.87	*	*	*	*	*
C_SHR	/	-0.75	-0.90	-1.04	-1.18	-1.31	/	/	/	/	/
A_SHR	/	-0.38	-0.45	-0.53	-0.60	-0.66	/	/	/	/	/
C4_GRA	-0.85	-0.71	-0.84	-0.97	-1.10	-1.22	0.83	0.99	1.14	1.29	1.44
C3_GRA	-0.62	-0.47	-0.55	-0.64	-0.73	-0.81	0.75	0.89	1.03	1.17	1.30
CRO	-3.35	-1.97	-2.57	-3.28	-4.11	-5.10	0.59	0.77	0.98	1.23	1.52
Fitting ^c	/	0.61	0.79	0.99	1.23	1.50	/	/	/	/	/
Median	/	/	/	/	/	/	0.74	0.88	1.01	1.20	1.37
							(0.72)	(0.86)	(0.99)	(1.17)	(1.30)
Std	/	/	/	/	/	/	0.19	0.21	0.23	0.25	0.28
							(0.09)	(0.08)	(0.07)	(0.08)	(0.13)

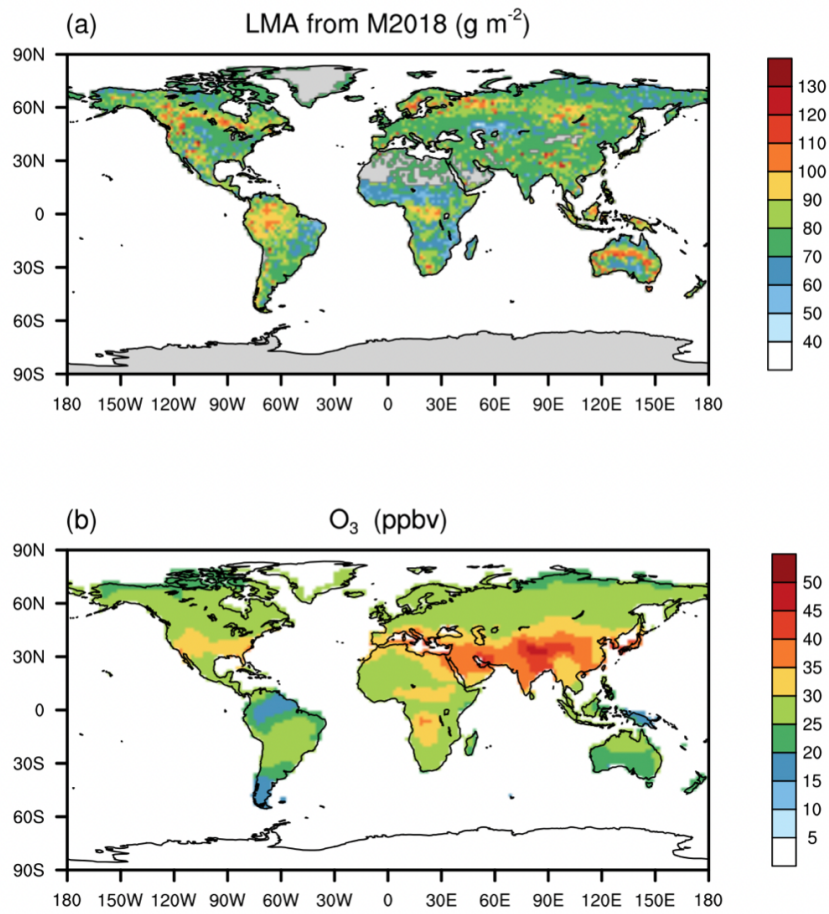
672

673 ^a All runs from the YIBs-LMA experiment use $x=0.019$ nmol g⁻¹ s⁻¹ and LMA map from M2018.674 ^b Slopes of simulated DRRs (S_s) are divided by observations (S_o , Table S1) to derive the model-to-observation ratios (“ S_s/S_o ”).675 O₃ dose metric is POD_{y=1} for natural PFTs and POD_{y=6} for crops. The Median and standard deviation (Std) of S_s/S_o ratios of676 all PFTs are calculated for each set of specific parameter *a*. The values in parentheses exclude the effect of those numbers

677 marked with * that are out of 1 standard deviation.

678 ^c The slopes (Fitting) of linear regressions between S_o and S_s are listed for each *a*. The optimal *a* with 1:1 fitting between S_s 679 and S_o is bolded.

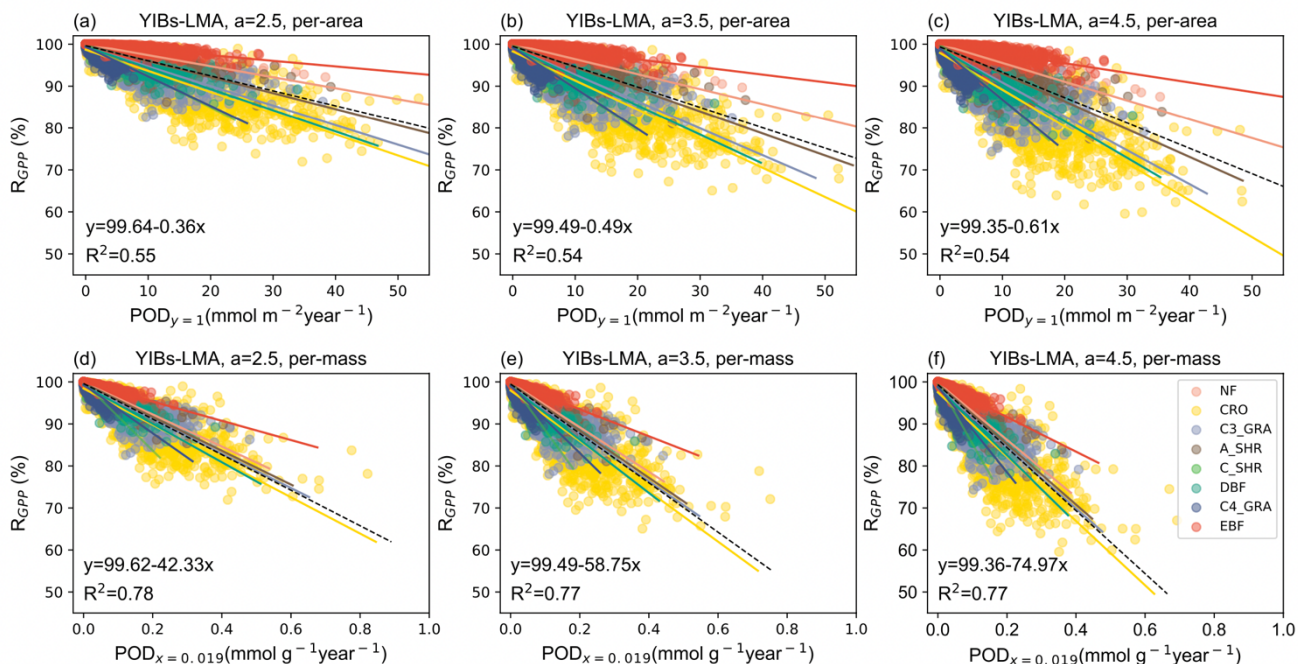
680



681

682 **Figure 1.** Global leaf mass per area (LMA) and surface ozone (O_3) concentrations. The (a) LMA is
683 adopted from Moreno-Martinez et al. (2018) (M2018) and (b) annual mean O_3 is derived from TF-HTAP
684 (Turnock et al., 2018).

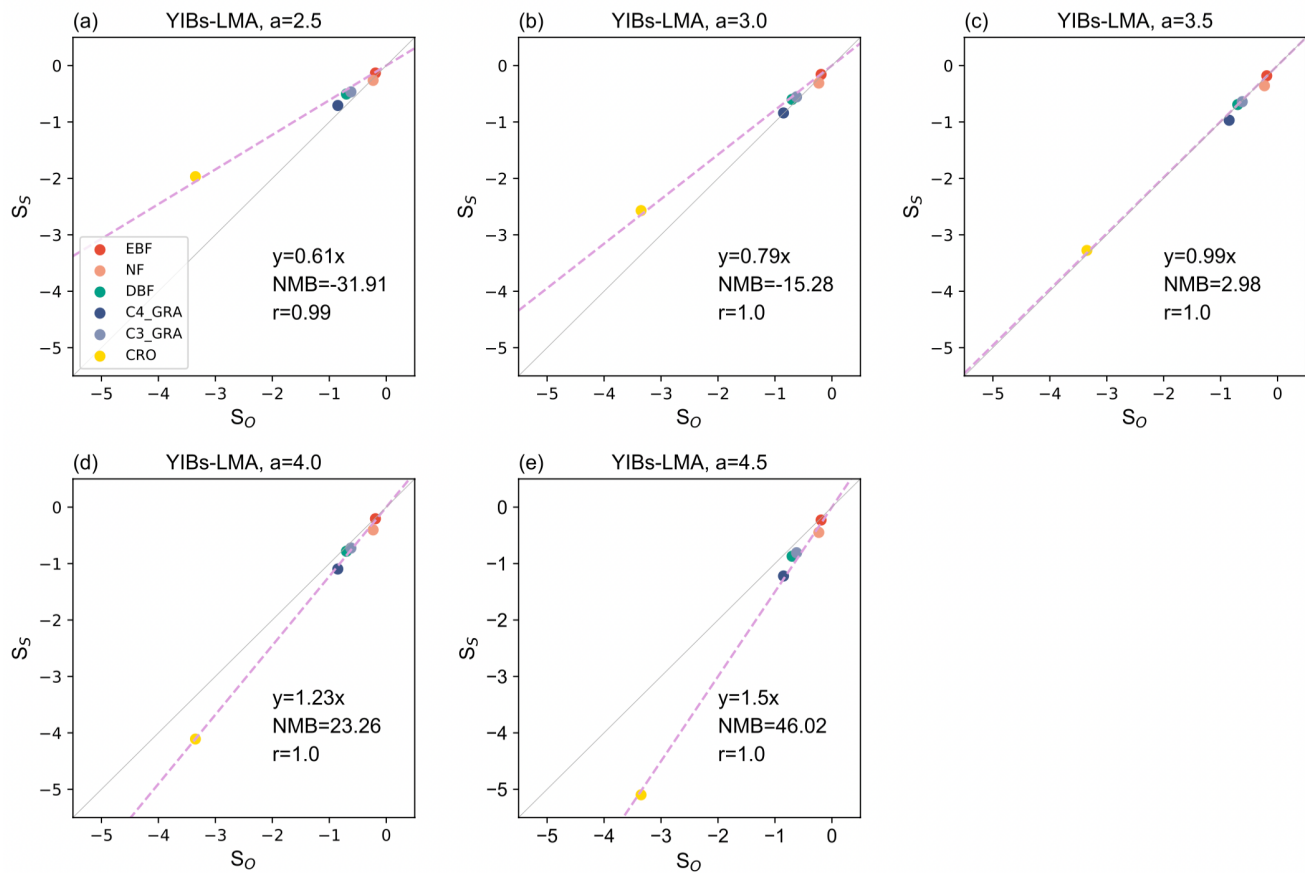
685



687

688 **Figure 2.** Simulated area-based (top) or mass-based (bottom) DRRs for the YIBs-LMA experiment.
 689 Three tests from the YIBs-LMA experiment all adopt $x=0.019$ nmol g⁻¹ s⁻¹ and gridded LMA from M2018
 690 with parameter $a=2.5, 3.5, 4.5$ nmol⁻¹ s g, respectively. Each dot represents estimated POD- R_{GPP} ($POD_{y=1}$
 691 for (a)-(c), $POD_{x=0.019}$ for (d)-(e)) at a grid with corresponding PFT. The PFT-specific regressions between
 692 area- or mass- based POD and R_{GPP} are displayed with solid lines shown in legend. Regression
 693 relationships of all PFTs are displayed in black dash line with coefficients of determination (R^2) denoted
 694 on each panel. Note the differences of ranges in x axis among PFTs. The YIBs-LMA experiment is
 695 summarized in Table 1.

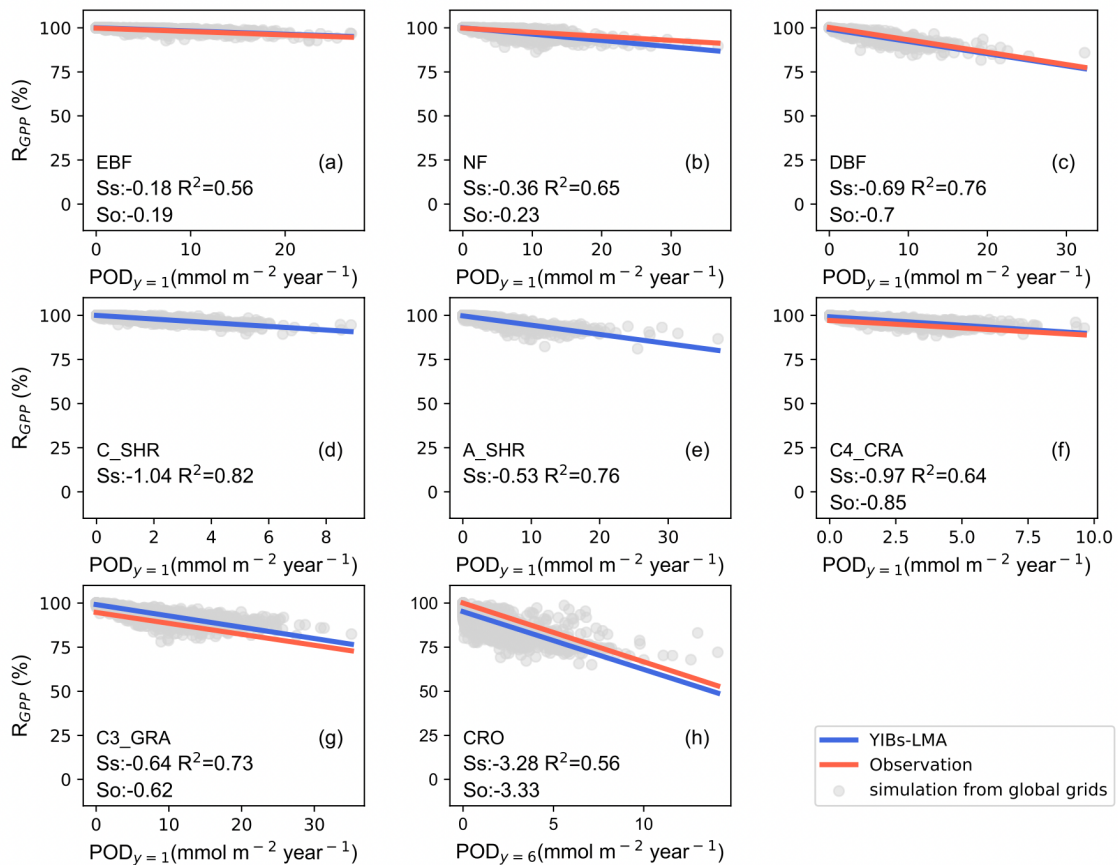
696



698

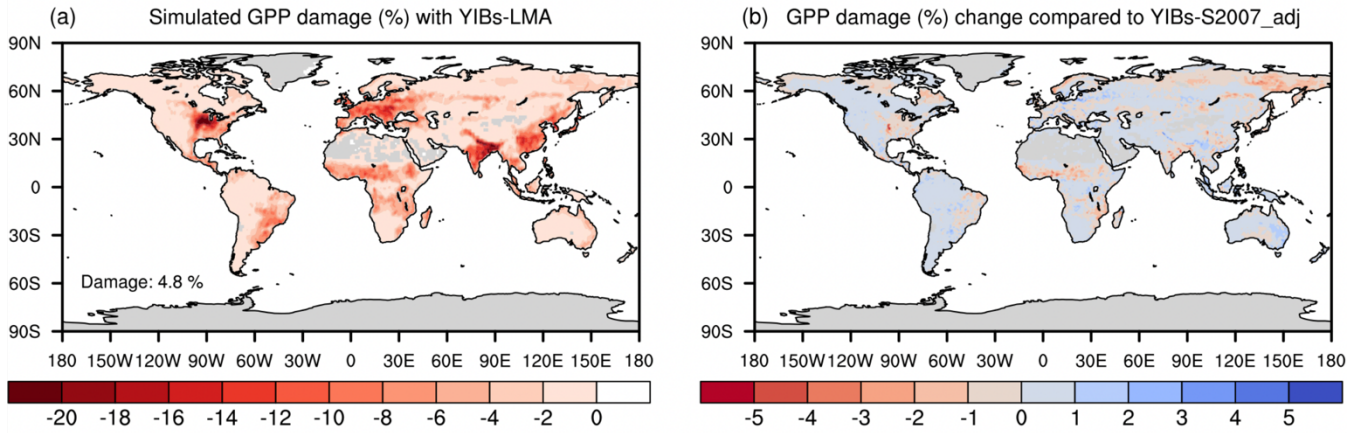
699 **Figure 3.** Comparison between S_O (% per mmol m^{-2}) and S_S (% per mmol m^{-2}) for the YIBs-LMA
700 experiment. Five tests from the YIBs-LMA experiment all adopt $\alpha=0.019 \text{ nmol g}^{-1} \text{ s}^{-1}$ and gridded LMA
701 from M2018 but with varied parameter a from (a) 2.5 to (e) 4.5 $\text{nmol}^{-1} \text{ s g}$. S_O are from Table S1. S_S are
702 derived as the slope between R_{GPP} and POD_y . The linear regression (dashed lines), 1:1 fitting (light grey
703 lines), normalized mean biases (NMB), and correlation coefficient (r) between S_S and S_O for varied PFTs
704 are shown on each panel. The S_S and S_O of CRO are derived using $\text{POD}_{y=6}$ while other PFTs use $\text{POD}_{y=1}$.
705 The YIBs-LMA experiment is described in Table 1.

706



707

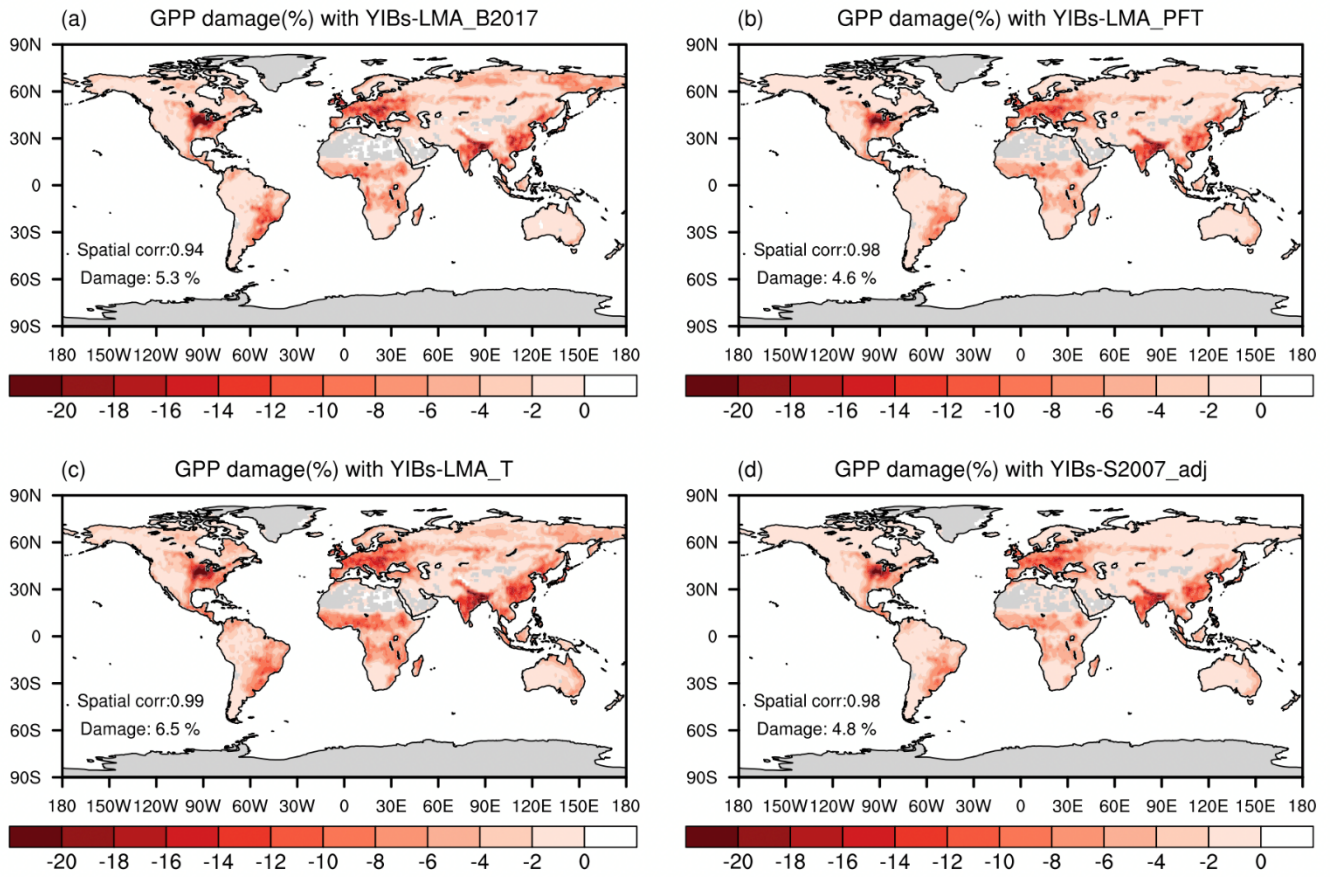
708 **Figure 4.** Comparisons of observed and simulated dose-response relationships. Simulated PFT-specific
 709 DRRs are derived from YIBs-LMA with gridded LMA from M2018, $x=0.019$ nmol g⁻¹ s⁻¹, and $a=3.5$
 710 nmol⁻¹ s g. Each dot represents results from a gridcell with corresponding PFT. The regressions between
 711 relative GPP percentage (R_{GPP}) and leaf area-based stomatal O_3 uptake fluxes ($POD_{y=1}$ for natural PFTs
 712 and $POD_{y=6}$ for crops) are shown for observations (red, see Table S1) and simulations (blue) with slopes
 713 of DRRs denoted as S_o and S_s , respectively. S_o are missing for (d) cold and (e) arid shrubs. Coefficients
 714 of determination (R^2) of simulations are displayed in each panel. Note the differences of ranges in x axis
 715 among PFTs (PFTs are shown in Fig. S1).



716

717 **Figure 5.** Global O₃ vegetation damage simulated with the LMA-based scheme. Results shown are the
 718 (a) GPP reduction percentages by O₃ simulated with the YIBs-LMA framework (gridded LMA from
 719 M2018, $x=0.019 \text{ nmol g}^{-1} \text{ s}^{-1}$, and $a=3.5 \text{ nmol}^{-1} \text{ s g}$), and (b) their differences compared to the predictions
 720 from YIBs-S2007_adj simulation. Blue (red) patches indicate the regions where damages predicted in
 721 YIBs-LMA are lower (higher) than those in YIBs-S2007_adj.

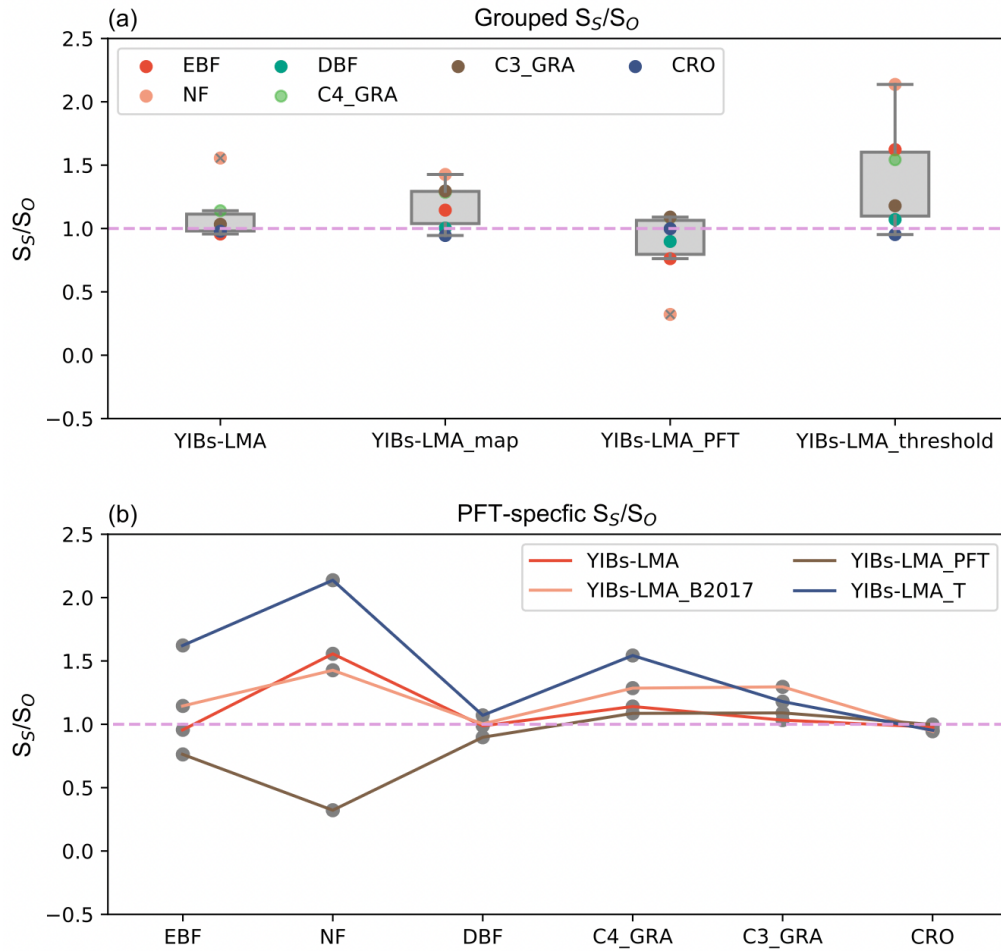
722



724

725 **Figure 6.** Global O₃-induced GPP reductions simulated in four supporting experiments. All damage maps
 726 are based on optimal parameters shown in Table 1. The spatial correlation coefficients between YIBs-
 727 LMA and these supporting simulations are shown on each panel as well as the global average damage
 728 percentage of each map. Simulations are described in Table 1.

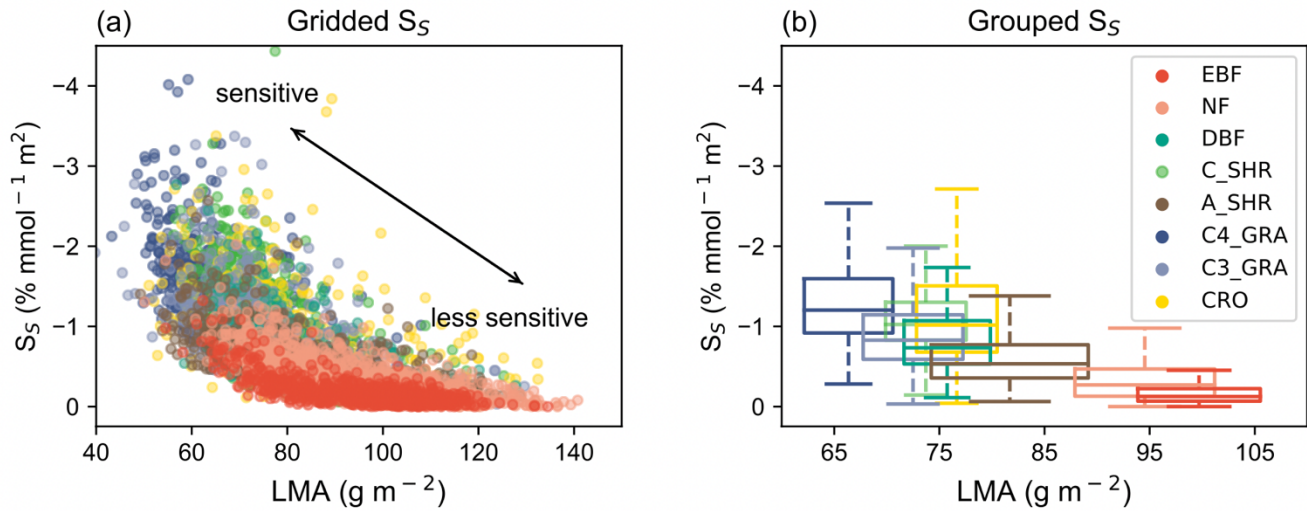
729



730

731 **Figure 7.** Comparison of S_S/S_O among supporting experiments. Individual ratios for (b) different PFTs
 732 are grouped to the boxplot in (a). All experiments adopt optimal parameters shown in Table 1.

733



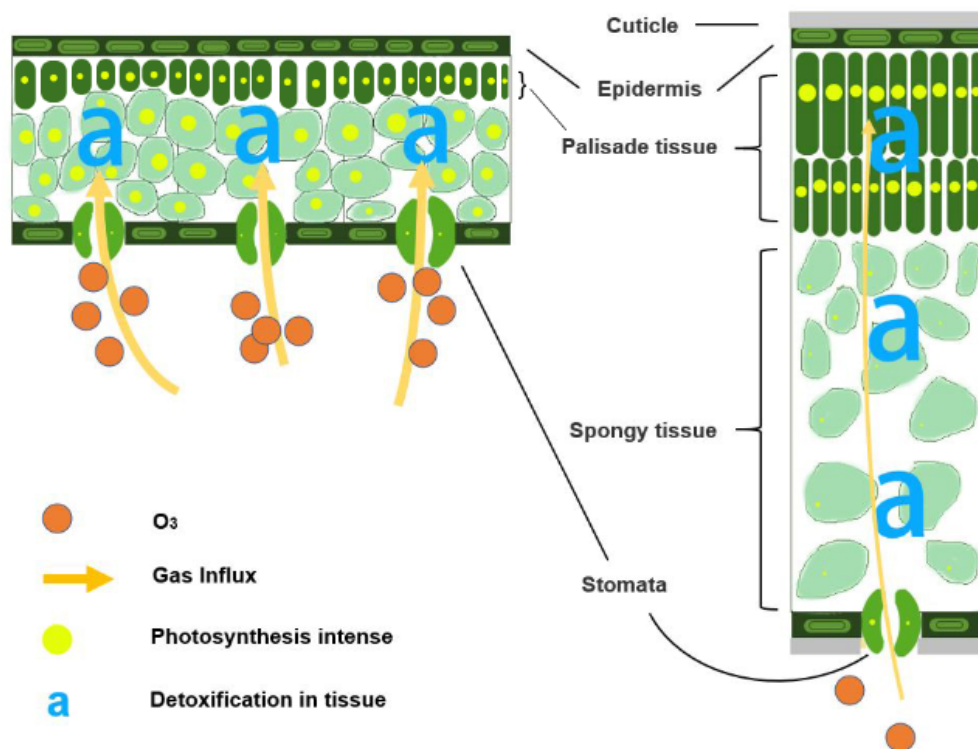
735

736 **Figure 8.** Relationships between O₃ sensitivity and LMA. (a) Simulated O₃ sensitivity (S_5) at each grid is
 737 compared with LMA for different PFTs. Gridded S_5 is derived as GPP change per unit $\text{POD}_{y=1}$ from the
 738 YIBs-LMA simulation. Each point represents the value in a grid cell with a dominant PFT. (b) The PFT-
 739 level relationships between LMA and O₃ sensitivity are grouped as boxplots, which indicate the median,
 740 25th percentile, and 75th percentile of y-axis variables within the same PFT. The width of boxplots
 741 represents one standard deviation of LMA for a specific PFT.

742

Mode1 : Sensitive, Fast

Mode 2 : Less-sensitive, Slow



743

744 **Figure 9.** Illustration of the relationships between leaf trade-off strategy and its sensitivity to O_3

745